Olabode, Olaitan; Kosunen, Marko; Halonen, Kari

A current controlled oscillator based readout front-end for neurochemical sensing in 65nm CMOS technology

Published in:
ISCAS 2016 - IEEE International Symposium on Circuits and Systems

DOI:
10.1109/ISCAS.2016.7527290

Published: 11/08/2016

Document Version
Peer reviewed version

Please cite the original version:
Olabode, O., Kosunen, M., & Halonen, K. (2016). A current controlled oscillator based readout front-end for neurochemical sensing in 65nm CMOS technology. In *ISCAS 2016 - IEEE International Symposium on Circuits and Systems* (pp. 514-517). [7527290] (IEEE International Symposium on Circuits and Systems). IEEE. https://doi.org/10.1109/ISCAS.2016.7527290

A Current Controlled Oscillator Based Readout Front-end for Neurochemical Sensing in 65nm CMOS Technology

Olaitan Olabode, Marko Kosunen and Kari Halonen
Department of Micro and Nanosciences
Aalto University School of Electrical Engineering, Espoo, Finland
Email: olaitan.olamilehin@aalto.fi

***Abstract*—This paper presents the design of an integrated current-controlled oscillator (CCO) based readout front-end for neurochemical sensing applications. The readout front-end chip is implemented in 65 nm CMOS technology and occupies an area of 0.059 mm^2. The proposed design supports an input current range of 1.2 μA (± 600 nA) and can also be configured to support wider current range. The CCO-based structure utilized in this design results in noise averaging of the detected neurochemical input signal due to its inherent $\Delta\Sigma$ first-order noise shaping and anti-alias filtering characteristics. Thus, the prototype chip achieves a current resolution of 100 pA and can detect dopamine concentrations as small as 10 μMol based on measured data from novel diamond-like carbon electrodes. In addition, the digital codes obtained from the readout front-end attain a signal-to-noise (SNR) of 82 dB and linearity limited effective-number-of-bits (ENOB) of 8 at full current range input, without employing any calibration or linearization techniques. The proposed read-out front-end consumes 33.7 μW of power in continuous operation.**

I. Introduction

Sensing and real-time monitoring of neural activities within the central nervous system (CNS) has become a fast-growing area of research due to the need to understand more about how neurons communicate as well as the emerging needs related to personalized healthcare and brain machine interfaces. In addition, further knowledge on how neurons transmit information within the CNS is of significant value to researchers in the field of neuroscience for improving treatment of neurological disorders and neurodegenerative diseases.

Neurons in the CNS are connected by synapses and communicate through electrical and chemical impulses or signals. Transmission of neurochemical signals occurs over short distances in the order of $(20-30)$ nm, across chemical synapses; as a result of discharge and absorption of biochemical molecules also known as neurotransmitters [1]. The region or gap between chemical synapses forms a chemical synaptic junction also known as synaptic cleft. The synaptic cleft is filled with an extracellular fluid which aids the chemical reactions that occur during neurochemical transmission. Neurochemical signals are responsible for controlling cognitive, learning and memory functions in the brain. Thus, several neurological disorders such as Parkinson's disease, Schizophrenia, Alzeihmers and Epilepsy have been reported to be associated with abnormal concentration levels of neurotransmitters such as glutamate and dopamine [2]. Hence, the readout and analysis of neurotransmitter concentration levels from the brain provides insight into neurochemical signalling and plays a vital role in the development of more effective treatments for patients suffering from neurological disorders.

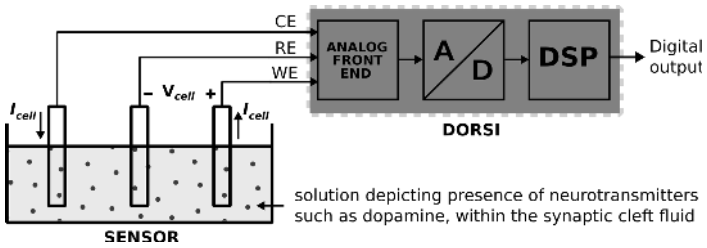

Fig. 1. System block diagram showing the interface between the proposed readout front-end (DORSI) and the neurochemical sensor electrodes which are designed to be implanted at chemical synaptic junctions in the brain.

Neurochemicals such as dopamine, histamine, norepinephrine, and serotonin; are primarily monitored with the help of potentiostats which operate based on electrochemical transduction principle [3]. Electrochemical transduction principle is the process of applying an electrical potential (V_{cell}) across an electrochemical cell and measuring the induced reduction-oxidation (redox) current within the cell (I_{cell}) as illustrated in Fig. 1. Thus, this paper proposes a readout front-end for the measurement of neurochemical induced currents based on redox reactions of neurotransmitters within the synaptic cleft. The detected current profiles from the readout chip (DORSI) represents change in concentration levels of neurotransmitters at the neurochemical sensor interface as depicted in Fig. 1. As a result, the detected oxidation and reduction peak potentials help to regulate the voltage applied by neurostimulation electrodes when used in deep-brain stimulation of patients suffering from dopamine-deficient disorders such as Parkinson's disease [4].

This paper is organized as follows; Section II describes the system level design of the proposed readout front-end. Section III presents post-layout simulation results based on measured data from the neurochemical sensor electrodes. Finally, performance of the proposed design is summarized in Section IV.

II. Proposed Design

The main challenge in the design of readout front-ends for neurochemical sensing is the required support of a wide range of input currents while achieving current resolution in pA or less range. Hence, the proposed design of the readout front-end is based on a mixed-signal architecture for minimizing

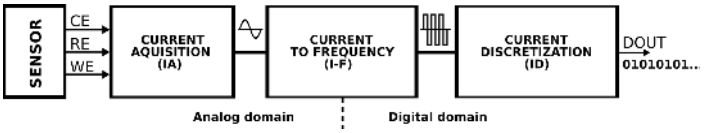

Fig. 2. Neurochemical signal processing stages in DORSI.

the effect of noise and achieving high resolution of detected current signals. In addition, sensitivity and selectivity of the sensor electrodes to neurochemicals play an important role in achieving good current resolution from the readout front-end. Thus, the novel diamond-like carbon electrodes used in this work ensures more stable detection of neurochemicals and provides lower background current (I_{bg}). The input signal is processed within the readout front-end along three main stages, across analog and digital domains as shown in Fig. 2. First, the neurochemical induced current is acquired in the IA stage. Then, the acquired current from the IA stage is converted to frequency in the I-F stage. Lastly, the pulses generated from the I-F stage are quantized in the ID stage such that the digital output from the readout front-end can be further processed by neurostimulation circuitry or externally outside the brain.

A. System Architecture

This section describes the internal structure of the proposed design and noise averaging technique of the current-controlled oscillator (CCO) based architecture. The induced cell current (I_{cell}) from the neurochemical sensor is processed in the IA stage in order to generate the control current (I_{ctrl}) for the I-F stage. Then, a simple RC-filter is applied to I_{ctrl} in order to limit the noise bandwidth. The low-pass filtered I_{ctrl} signal is conveyed to the CCO which converts the current signal to frequency domain with I-F conversion gain (K_{cco}) as illustrated in Fig. 3. Thus, the frequency of the oscillator (F_{cco}) is modulated by changes in the detected input current. The frequency-domain information at the output of the I-F gain stage is integrated to generate changes in phase domain $\phi_{cco}(t)$. Hence, the continuous change in the phase of signal $x(t)$ is quantized to the amplitude domain in the ID stage with an integrate-and-dump algorithm.

The quantizer is implemented as an up-counter which is triggered at the rising edge of the generated pulses from the CCO. In addition, the accumulated counter codes ($\Sigma_{(\phi)}$) at the output of the quantizer are sampled to generate discrete representation of the accumulated phase change $\phi[n]$. As a result, the ID stage is controlled by two clocks namely; F_{cco} and F_s, which divides the ID block into increment and readout clock domains respectively. The increment clock domain is controlled by an asynchronous clock from the CCO since F_{cco} varies with changes in I_{cell}. On the other hand, the readout clock domain is controlled by a fixed sampling clock F_s which synchronizes subsequent processing by the discrete-time derivator and determines the effective data output rate of the system. Hence, the counter utilizes gray-coding in order to mitigate the effect of possible timing violations that may occur at the clock domain crossing (CDC) between the two clock domains as depicted in Fig. 3. In addition, the use of gray-code counters ensures that the minimum error due to possible metastability in the digital circuitry is limited to 1 LSB.

Furthermore, the discrete-time phase sampler defines the

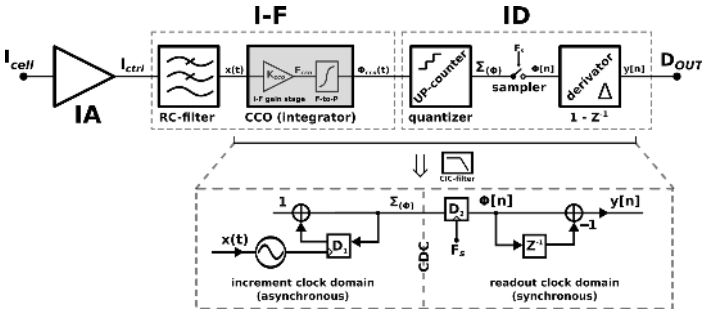

Fig. 3. Electrochemically induced cell current life-cycle within DORSI.

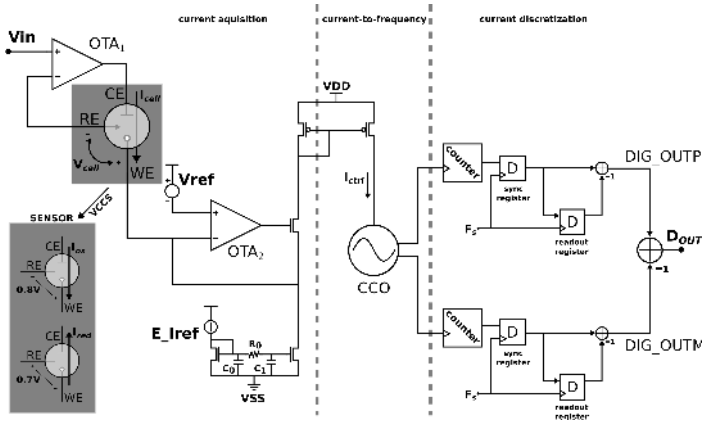

Fig. 4. Top-level schematic of the readout front-end (DORSI).

integration time (T_s) of the changes in phase and the output of the sampler $\phi[n]$ is differentiated in order to obtain the digital output codes (D_{OUT}). Hence, the CCO-based analog-to-digital (A/D) conversion with integrate-and-dump digital interface results in a cascaded-integrator-comb (CIC) filter which has a continuous-time *sinc* frequency response. As a result, the integrate-and-dump structure effectively averages the noise over the sampling interval T_s and prevents aliasing of wide-band noise into the signal band [5]. Thus, the frequency response of this system is given as follows with images on integer multiples of F_s [6].

$$[H(f)] = \frac{K_{cco} * sin\left(\frac{\pi * f}{F_s}\right)}{\pi * f} \tag{1}$$

$$\Rightarrow [H(0)] = \frac{K_{cco}}{F_s} = K_{cco} * T_s \tag{2}$$

B. Circuit Level Design

This section describes the system level design of the readout front-end and circuit implementations of each signal processing stage of the proposed design. Fig. 4 presents the top-level schematic of the readout front-end based on the system architecture described in the previous Section II-A. The following sub-sections elaborate on the design of each processing block in the system.

1) Current Acquisition (IA): This block represents the analog front-end of the system and controls the cell voltage (V_{cell}) that is applied across the working electrode (WE) and

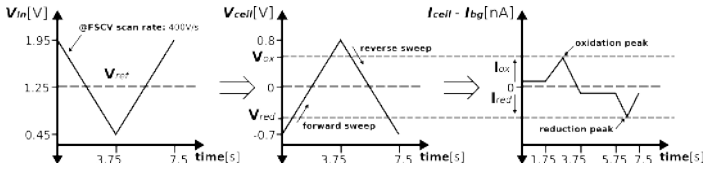

Fig. 5. Relationship between V_{in}, V_{ref}, V_{cell}, I_{cell} and I_{bg}.

reference electrode (RE) of the neurochemical sensor as shown in Fig. 1. The applied V_{cell} is controlled based on fast-scan cyclic voltammetry (FSCV) sweep of the input voltage (V_{in}) in order to acquire the induced cell current (I_{cell}) flowing between the counter electrode (CE) and WE. Thus, this block is designed to provide stable V_{cell} between -0.7 V to 0.8 V in order to detect oxidation (I_{ox}) and reduction (I_{red}) current peaks of neurochemicals during the forward and reverse sweep of the input voltage as depicted in Fig. 5. As a result, the FSCV requirements for V_{in} range of 1.5 V, limits the minimum supply voltage and defines the input common-mode range (ICMR) requirements of the operational transconductance amplifiers (OTAs). The OTAs are designed using the conventional Miller OTA architecture and can operate with supply voltage between 1.8 V and 2.5 V. In addition, the OTA is designed to provide high gain of 80 dB in order to minimize DC offsets and gain errors, which in turn ensures stable and accurate control of V_{cell}. Furthermore, the structure of the IA stage is based on a transimpedance topology where OTA_1 and OTA_2 are operating in a voltage follower configuration for setting the voltage at RE and WE respectively, which in turn sets V_{cell} as follows.

$$V_{cell} = V_{WE} - V_{RE} = V_{ref} - V_{in} \tag{3}$$

$$\Rightarrow I_{cell} = \frac{V_{cell}}{Z_{cell}} = \frac{V_{ref} - V_{in}}{Z_{cell}} \tag{4}$$

The neurochemical sensor is presented in Fig. 4 as an electrochemical cell and can be modelled as a voltage-controlled current source (VCCS) which exhibits non-linear resistance based on changes in the neurochemical concentration levels. Hence, the acquired cell current is defined as the ratio of the applied V_{cell} to the total impedance of the cell (Z_{cell}) as expressed in equation (4). The reference current (E_I_{ref}) is used to define the control current I_{ctrl} of CCO such that the acquired redox current I_{cell} is added to or subtracted from E_I_{ref} as described in the following equation.

$$I_{ctrl} = E\_I_{ref} \mp I_{cell} \tag{5}$$

As a result, I_{ctrl} is a positive value that decreases or increases from the defined reference current E_I_{ref}. Thus, E_I_{ref} can be configured to support a wide range of input current. In addition, the reference current E_I_{ref} can also be reduced if the detected current range from the neurochemical of interest is low, in order to reduce power consumption. The IA block occupies an area of 0.019 mm^2 and draws an average current of 6.64 μA from 1.8 V supply.

2) Current-to-Frequency (I-F): This block crosses both analog and digital domains as depicted in Fig. 2, since it performs the initial A/D conversion of the varying current signal to frequency. Thereby providing as an output, phase representation of the continuous-time analog signal which serves as an input to the ID stage. As a result, this block performs continuous-time sampling of the analog signal in frequency domain and the ID block implements further processing of the sampled signal such as quantization and discrete-time sampling. Hence, this block and the ID block make-up a CCO-based ADC for the readout front-end.

In addition, this block is implemented as a differential CCO based on two single-ended ring oscillators where each oscillator has three current starved inverter stages and two output buffer stages. The inverter stages are controlled by I_{ctrl} and the bias current of the oscillator (O_I_{ref}). Hence, the operating frequency (F_{cco}) range of this block can be tuned by adjusting O_I_{ref} of the CCO. Furthermore, the frequency outputs of the differential CCO are complementary to each other and when subtracted from each other, the attained I-F sensitivity is twice that of a single oscillator. Hence, the differential operation of the CCO improves the linearity of the I-F conversion and increases the conversion gain, which in turn improves the resolution attained from the ID stage. The I-F block occupies an area of 0.005 mm^2 and draws an average current of 10.46 μA from 1 V supply.

3) Current Discretization (ID): This block performs digital signal processing (DSP) functions such as noise averaging and encoding of the digital codes (D_{OUT}). Noise averaging is achieved over a long integration time (T_s) of the pulses from the I-F block followed by discrete-time sampling and derivation as discussed in Section II-A. Hence, the data rate of the system is defined by the sampling frequency (F_s) of this block which is limited by the signal bandwidth. In addition, the current-to-digital code conversion gain of this block is defined by F_{cco} and F_s based on the number of pulses or phase transitions (N_p) within each sampling interval T_s, where N_p changes as F_{cco} is modulated by I_{cell}. Therefore, tunability of the F_{cco} range offers flexible control of the dynamic range (DR) and digital code resolution (n) of the system as shown in the following equations based on equation (2). However, the maximum F_{cco} tuning range is limited by non-linearity of the CCO which significantly degrades the effective-number-of-bits (ENOB) of the ADC [5].

$$Dynamic\ range\ (DR) \approx \frac{F_{cco}(max) - F_{cco}(min)}{F_s} \tag{6}$$

$$\Rightarrow Resolution\ (n) \approx log_2\,(DR) \tag{7}$$

Finally, it should be noted that the derivation stage is evaluated off-chip during post-processing in Matlab. The ID block occupies an area of 0.035 mm^2 and draws an average current of 11.2 μA from 1 V supply.

III. Post-layout simulation results

The readout front-end is implemented in 65 nm CMOS technology and Fig. 6 shows the layout of the fabricated chip. Fig. 7 shows the performance of the I-F and ID blocks based on acquired I_{cell} from the IA block. The I-F block and the ID block achieve current sensitivity of 13 kHz/nA and 100 pA/LSB respectively. The I-F block is optimized to provide 16 MHz frequency range from the differential CCO as shown in Fig. 7a, but it should be noted that the current sensitivity of the I-F block can be increased by tuning the CCO to provide wider frequency range. Fig 7b shows that 13.3-bits digital code resolution was obtained from the ID block which could be further increased by reducing the sampling frequency. Fig. 8

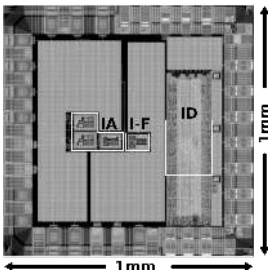

Fig. 6. Layout of the readout front-end chip implemented in 65 nm CMOS

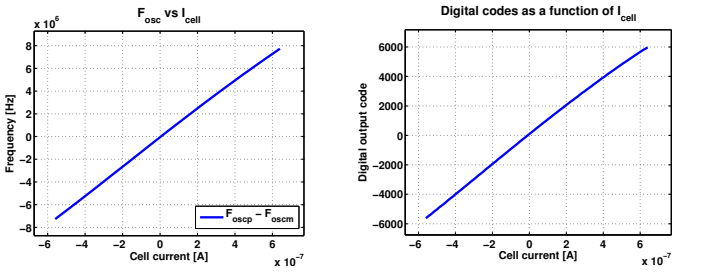

(a) $OSC\_OUTP - OSC\_OUTM$ (b) $DIG\_OUTP - DIG\_OUTM$

Fig. 7. (a) I-F sensitivity of the CCO and (b) represents corresponding digital codes D_{OUT} from the ID block based on I_{cell} range of 1.2μA.

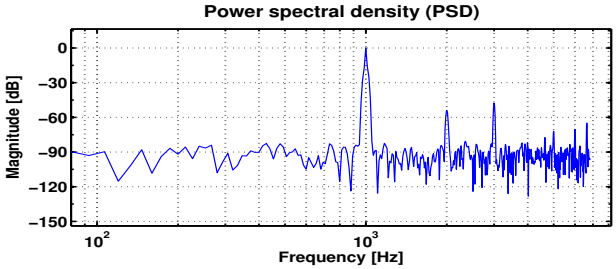

Fig. 8. FFT analysis of the digital output codes with 1 kHz and $\pm$0.8 V sine wave input which corresponds to full input current range of $\pm$600 nA.

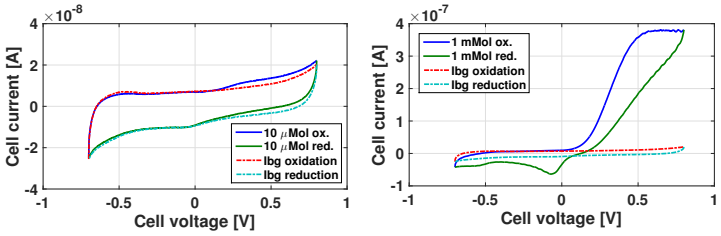

(a) 10 μMol of dopamine (b) 1 mMol of dopamine

Fig. 9. Simulation of detected cell current (I_{cell}) and background current (I_{bg}) based on FSCV dopamine measurements from the sensor electrodes.

presents the power spectral density of the digital codes from the ID block where the achieved SNR is 82 dB and SFDR is 50 dB, which corresponds to an ENOB of 8-bits. The significant difference between the SNR and SFDR is due to the known effect of inherent frequency tuning non-linearity of oscillator based ADCs [5]. Nonetheless, the achieved resolution provides good sensitivity for neurochemical applications as shown in the simulation results presented in Fig. 9 and Fig. 10 based on dopamine measurements with FSCV scan rate of 400 V/s.

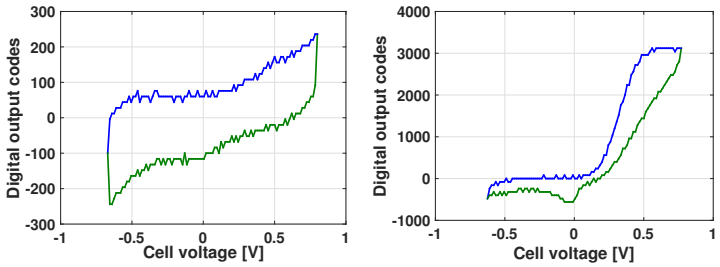

(a) 10 μMol of dopamine (b) 1 mMol of dopamine

Fig. 10. Corresponding digital codes from the readout front-end based on detected cell currents for the dopamine concentrations shown in Fig. 9.

IV. Conclusion

The readout of concentration levels of neurochemicals from the brain contributes to the realization of fully-implantable closed-loop interfaces for stimulation of degenerative neurons and control of neural activities. This paper described the design of a CCO-based readout front-end for neurochemical sensing applications. The proposed design was implemented in a 65 nm CMOS process. Post-layout simulation results shows that the readout front-end provides current resolution of 100 pA and could detect minimum dopamine concentration of 10 μMol based on measured data from novel diamond-like carbon electrodes. Higher and lower dopamine concentration than 10 μMol can also be detected from the readout front-end due to its support for a wide current range of 1.2 μA($\pm$600 nA). The digital code representation of the detected dopamine has a resolution of 13.3-bits with RMS conversion error of 0.18 LSB which results in an SNR of 82 dB at full current range input. The achieved resolution of the readout front-end provides good sensitivity of released neurochemicals in the brain which is useful for further understanding of neurotransmitters and fostering research into improved treatments of related neurodegenerative diseases.

Acknowledgment

The authors would like to thank Academy of Finland and Aalto University for funding this research work.

References

[1] R. K. Goyal and A. Chaudhury, "Structure activity relationship of synaptic and junctional neurotransmission," *Autonomic Neuroscience*, vol. 176, no. 1-2, pp. 11–31, 2013.

[2] J. M. Beaulieu and R. R. Gainetdinov, "The physiology, signaling, and pharmacology of dopamine receptors," *Pharmacological reviews*, vol. 63, no. 1, pp. 182–217, Mar 2011.

[3] M. Roham, D. Covey, D. Daberkow, E. Ramsson, C. Howard, B. Heidenreich, P. Garris, and P. Mohseni, "A Wireless IC for Time-Share Chemical and Electrical Neural Recording," *IEEE Journal of Solid-State Circuits*, vol. 44, no. 12, pp. 3645–3658, Dec 2009.

[4] K. H. Lee, C. D. Blaha, P. A. Garris, P. Mohseni *et al.*, "Evolution of Deep Brain Stimulation: Human Electrometer and Smart Devices Supporting the Next Generation of Therapy," *Neuromodulation: Technology at the Neural Interface*, vol. 12, no. 2, pp. 85–103, 2009.

[5] S. Rao, K. Reddy, B. Young, and P. Hanumolu, "A deterministic digital background calibration technique for VCO-based ADCs," *IEEE J. Solid-State Circuits*, vol. 49, no. 4, pp. 950–960, 2014.

[6] V. Unnikrishnan and M. Vesterbacka, "Time-mode analog-to-digital conversion using standard cells," *IEEE Transactions on Circuits and Systems I: Regular Papers*, vol. 61, no. 12, pp. 3348–3357, Dec 2014.